JOURNAL OF FORENSIC SCIENCES

J Forensic Sci, July 2012, Vol. 57, No. 4
doi: 10.1111/j.1556-4029.2012.02082.x
Available online at: onlinelibrary.wiley.com

CASE REPORT

ENGINEERING SCIENCES

Chan-Seong Park,[1] *Ph.D.; Seung-Won Jeon,*[2] *M.E.; Kyu-Jung Lee,*[2] *Ph.D.; Jun-Suk Kim,*[3] *M.E.; Jae-Geun Oh,*[1] *Ph.D.; Jong-Chan Park,*[4] *Ph.D.; Hong-Seok Lee,*[4] *Ph.D.; and Young-Shik Choi,*[1] *Ph.D.*

Wind-Drag Estimation in a Traffic Accident Involving a Motor Scooter and a Tractor–Trailer

ABSTRACT: This case report describes a noncontact traffic accident involving a motor scooter and a tractor–trailer with a focus on the wind-drag effect. We used load cells to measure the drag force acting on a substantially similar motor scooter when a substantially similar tractor–trailer passes by it, taking into consideration various speeds of the tractor–trailer and distances between the two vehicles. A three-dimensional steady-state flow analysis was also performed by using the CFX program for computational fluid dynamics to examine the streamlines and the pressure distribution around the tractor–trailer at various speeds. From the experiment, for a separation distance of 1.0 m (3.28 ft) and a speed of 90 km/h (55.9 mph), the maximum resultant drag force is 124.5 N (28 lb); this constitutes a degree of force that could abruptly disrupt the stability in maneuvering by an operator who is unaware of the approaching tractor–trailer. In addition, a single equation that relates the tractor–trailer speed to the drag force that acts on the motor scooter was derived on the basis of the Reynolds number (Re) and the wind-drag coefficient (C_d): $C_d = 1.298 \times 10^{-7}$ Re.

KEYWORDS: forensic science, traffic accident, wind-drag coefficient, Reynolds number, flow analysis, CFX

The speed limit of vehicles was recently increased in Korea under consideration of improved vehicle performance. The speed limit on city roads was increased from 60 km/h (37.3 mph) to 70 km/h (43.5 mph), and an increase from 100 km/h (62.1 mph) to 120 km/h (74.6 mph) for highways is currently being debated at length. In order to make changes to the speed limit for roads having narrow lanes, it is also imperative to consider pedestrian, bicycle, and motorcycle traffic, which can be influenced directly by the speed of vehicles via wind-drag, especially in the case of children and the elderly. This case report describes a noncontact traffic accident involving a motor scooter and a tractor–trailer with a focus on the wind-drag effect.

Case Report

A motor scooter operator lost control of the vehicle upon being passed by a tractor–trailer. There were no tire marks on the road reflecting physical signs of an accident (1). Figure 1 shows the position of the motor scooter in a series of time-lapsed photographs, which were recorded by CCTV installed at a gas station near the scene of the accident. The motor scooter was found in the opposite lane, near the center line. Because of poor image quality, contact or an impact between the tractor–trailer and the motor scooter could not be found. However, the speed of the tractor–trailer was estimated to be 70–80 km/h (43.5–49.7 mph). Figure 2 shows the tractor–trailer and the motor scooter; there was no evidence of contact. Among the various potential causes of the motor scooter crash, the wind-drag effect was deemed the primary focus, because the motor scooter crashed upon being passed by the tractor–trailer, as viewed from the recorded CCTV.

In fluid dynamics, drag, sometimes referred to as air resistance or fluid resistance, denotes the forces that oppose the relative motion of an object through a fluid. Drag forces act in a direction opposite to the oncoming flow velocity (2). As the tractor–trailer passes by the motor scooter, the flow field produced by the tractor–trailer movement affects the motor scooter via drag force. Considering two-dimensional flow fields by neglecting the flow directed upward, as it is relatively small compared with the flow in other directions, the drag force is considered to be the resultant force from two perpendicular forces in two directions.

The drag coefficient, C_d, is defined as:

$$C_d \equiv \frac{F_d}{\frac{1}{2}\rho V^2 A} \quad (1)$$

where F_d is the drag force; ρ, the density; V, the velocity; and A, the cross-sectional area. From Eq. (1), it can be seen that the magnitude of the drag force is a direct function of the speed of the tractor–trailer.

Many studies have been conducted on the aerodynamics of passenger vehicles and trucks, and these studies can be divided into two groups. The first group focuses on drag force reduction to improve fuel economy. Here, the aerodynamics of vehicles have

[1]Central District Office of National Institute of Scientific Investigation, Daejeon 305-348, Korea.
[2]Division of Mechanical Engineering, Korea University, Seoul 136-701, Korea.
[3]Division of Document and Image Analysis, National Institute of Scientific Investigation, Seoul 158-707, Korea.
[4]Division of Traffic Engineering, National Institute of Scientific Investigation, Seoul 158-707, Korea.

Received 18 May 2010; and in revised form 2 May 2011; accepted 4 June 2011.

FIG. 1—*The position of the motor scooter (dashed lines) in a series of time-lapsed photographs recorded by a CCTV installed at the gas station near the scene of the accident. The arrow indicates the location where the motor scooter crashed.*

FIG. 2—*(a) The tractor–trailer. There was no evidence of contact. (b) The motor scooter. There was no evidence of contact.*

been studied by numerical analyses using computational fluid dynamics or wind tunnel experiments (3–6). The second group focuses on the effect of wind or vehicle-induced airflow on vehicle stability or external objects such as pedestrians or other vehicles (7–13). Notable studies in this group include an investigation into the effect of wind on an emergency vehicle and on a tractor–trailer on a bridge, and the authors suggested safe wind speeds for the operation of such vehicles to prevent course deviation and overturning (7,8). The transient aerodynamic phenomena associated with a passing vehicle or series of vehicles were also studied (9–12). These studies suggested that significant interactions occur when the passing vehicle is within a distance corresponding to the length of the other vehicle, and there is a characteristic intervehicle spacing at which the drag of the rear vehicle is significantly increased. A simple analytical model for train-induced flow and its effects on pedestrians was developed (13). The authors of this work used unsteady potential theory to derive an analytical expression of the force exerted on a pedestrian. However, the theory has limited application, because it employs a simplified pedestrian and train model. No attempts have been made to quantitatively measure the loads imposed on a motor scooter by vehicle-induced gusts, as in the present case study.

TABLE 1—*Specifications of the tractor–trailer and the motor scooter.*

	Tractor	Trailer	Motor Scooter
Manufacturer	Scania	Incheon Motors	Hyosung Motors
Model	P380	ICDT-18DA	Super Cab
Year	2003	2004	2000
Overall length (ft)	22.3	26.0	5.7
Overall width (ft)	8.2	8.1	2.2
Overall height (ft)	10.2	10.1	3.4
Wheel base (ft)	14.6	4.4	4.0
Empty weight (lb)	18,982	12,125	163

In this study, the drag force acting on a substantially similar motor scooter when a substantially similar tractor–trailer passed by was experimentally measured using universal compression and tension-type load cells. Table 1 shows the specifications of the tractor–trailer and the motor scooter used for the experiments. Figure 3 shows the experimental setting of the motor scooter with the dummy operator. The motor scooter and the dummy operator were installed on rigid frames that were fixed to the ground. Two rigid rods, each equipped with a load cell, were used to attach the motor scooter to the frame, and were fixed to the center of mass of the motor scooter and the dummy operator (14). The dummy was fixed to the saddle of the motor scooter, and the weight was set to 60 kg (132 lb). One rod with a load cell was installed in the direction of the motor scooter movement, viz., the y direction, and the other rod with a load cell was attached in the direction of the left-hand side, viz., the x direction. Ball bearings were installed on each rod to prevent bending moments. The measured data on the drag force were stored on a computer through a data logger. The speed of the tractor–trailer was varied from 60 km/h (37.3 mph) to 90 km/h (55.9 mph), and the distance between the tractor–trailer and the motor scooter carrying the dummy was varied from 1.0 m (3.28 ft) to 2.0 m (6.56 ft). The experiment was performed along a straight road where the tractor–trailer could accelerate and steadily maintain the test speed. Figure 4 shows a photograph of the test site and the experimental apparatus.

A three-dimensional steady-state flow analysis was also performed using the CFX program for computational fluid dynamics to examine the streamlines and the pressure distribution of the tractor–trailer at various speeds (15). For simplicity, the computational domain was modeled for a tractor–trailer fixed to the ground under a steadily passing airflow corresponding with the speed of the tractor–trailer. In previous numerical studies on the aerodynamics of

heavy trucks or tractor–trailers, researchers used a full-scale tractor–trailer or truck model and considered an asymmetrically shaped tractor–trailer (3), the cross-wind (7), and unsteady airflow around the tractor–trailer (5,9,12), which result in asymmetric flow conditions for the tractor–trailer. Assuming that the tractor–trailer has a symmetric geometry with respect to the lateral direction and that air flows uniformly along the longitudinal direction of the tractor–trailer at the inlet boundary condition, a symmetric airflow condition results. Accordingly, half the tractor–trailer was modeled in this study for simplicity.

The κ-ε turbulent model, which provides computational accuracy (3–5,7,9,12), was used for the airflow analysis. The κ-ε turbulent model uses the gradient diffusion hypothesis to relate the Reynolds stresses to the mean velocity gradients and the turbulent viscosity. κ is the turbulent kinetic energy and is defined as the variance of the fluctuations of velocity. ε is the turbulent eddy dissipation and is the rate at which the velocity fluctuations dissipate (15).

Tetra-prism-type meshes were used for the solid wall of the tractor–trailer. Tetra mesh alone is not efficient for capturing shear or boundary layer physics. Hence, a prism mesh that efficiently captures these effects near the solid surface was also used (15). After a grid-dependence study, unstructured meshes with 2,514,454 nodes (3,576,355 elements) were used for the computations, as they yield more accurate results than other approaches (3–5,7,9,12). The convergence criteria for the root mean squared (rms) residual were set to 1E-6. The rms residual, $R(\omega)$, is the square root of the average of the squares of $\dot{\omega}$ in each cell of the domain. ω is the rate change of the conserved variable, $\dot{\omega}$, at every time step or iteration step (15):

$$R(\omega) \equiv \sqrt{\sum (\dot{\omega})^2}, \dot{\omega} = \frac{\partial \omega}{\partial t} \tag{2}$$

The boundary conditions were the mass flow at the inlet and the total pressure at the outlet, as generally adopted in previous studies (3–5,7,9,12). Air at 20°C (68°F) was considered as the working fluid, and the thermo-physical properties of the working fluid were

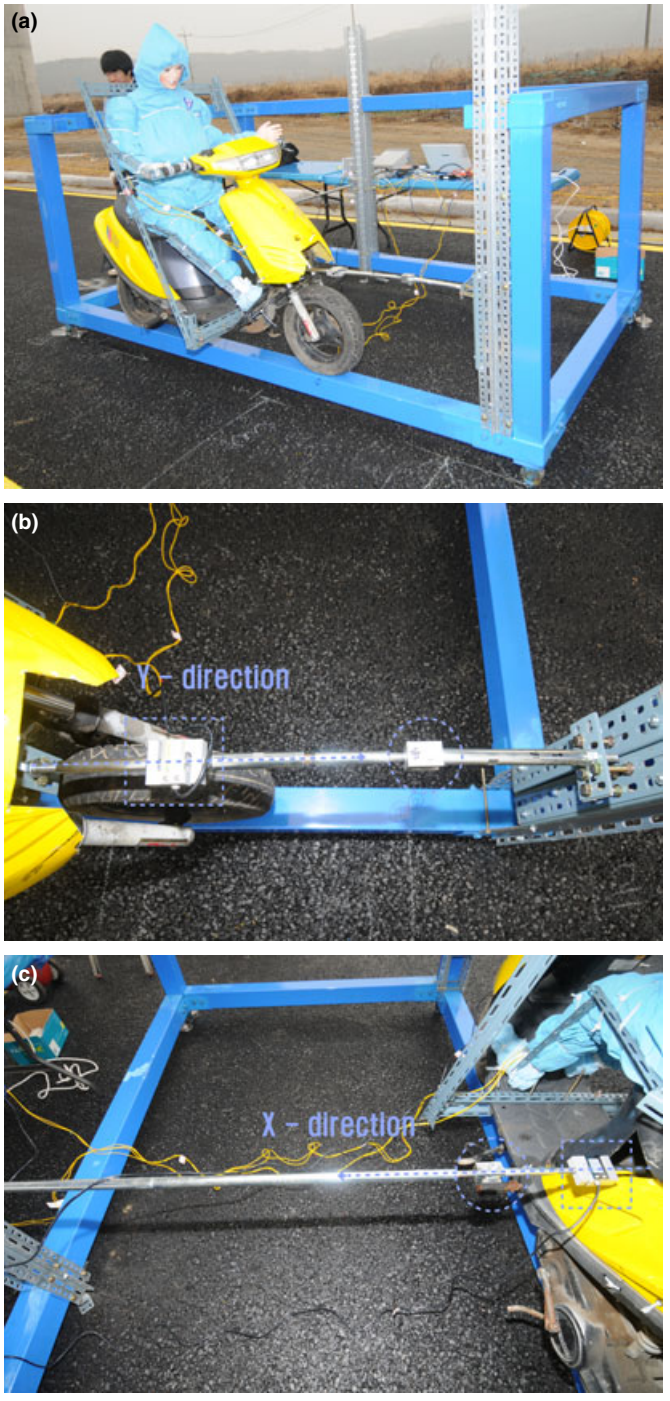

FIG. 3—*(a) Photograph of the experimental setup. The motor scooter and the dummy operator were installed on rigid frames that were fixed to the ground. Two rigid rods, each equipped with a load cell, were used to attach the motor scooter to the frame and were fixed to the center of mass of the motor scooter and the dummy operator. (b) Measurement of the* y*-directional force. The dashed rectangle indicates the load cell; the dashed circle indicates the ball bearing. (c) Measurement of the* x*-directional force. The dashed rectangle indicates the load cell; the dashed circle indicates the ball bearing.*

FIG. 4—*Photograph of the test site. The experiment was performed along a straight road where the tractor–trailer could accelerate and steadily maintain the test speed.*

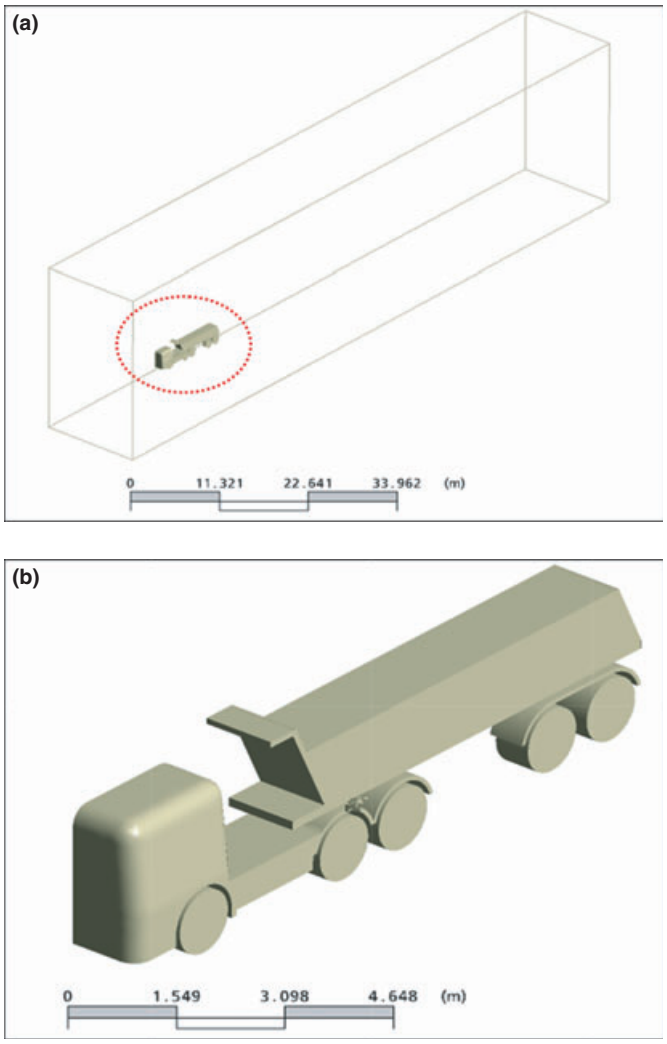

FIG. 5—*(a) Schematic illustration of the computational modeling. For simplicity, the computational domain was modeled for a tractor–trailer fixed to the ground while airflow steadily passed at the speed of the tractor–trailer. Dashed circle indicates the modeled tractor–trailer [see (b)], and solid lines indicate the computational domain. (b) The modeled tractor–trailer: considering symmetry, half the tractor–trailer was modeled.*

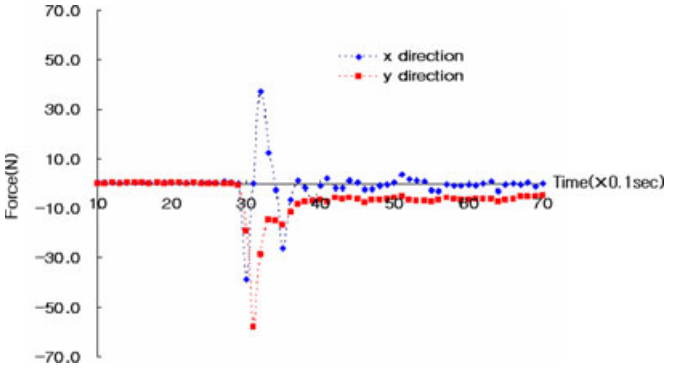

FIG. 6—*Example of the measured forces in the case of a tractor–trailer speed of 90 km/h (55.9 mph) and distance of 1.0 m (3.28 ft) between the two vehicles. As the tractor–trailer passed by, a compression force, that is, an airflow force on the motor scooter in the x* and *y directions, acted on the motor scooter carrying the dummy.*

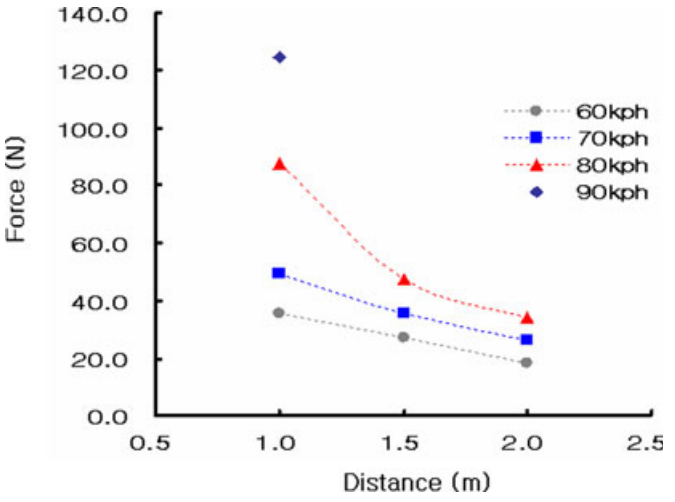

FIG. 7—*The maximum resultant forces. The resultant forces almost linearly increased at low speeds as the distance decreased. As the speed increased to 80 km/h (49.7 mph) or higher, the resultant forces increased steeply as the distance decreased.*

considered to be constant. Figure 5 presents a schematic illustration of the computational modeling.

Results and Discussion

Figure 6 shows an example of the measured forces in the case of a tractor–trailer speed of 90 km/h (55.9 mph) and distance of 1.0 m (3.28 ft) between the two vehicles. The measured data were saved on a computer at 0.25 sec intervals through a data logger. As the tractor–trailer passed by, a compression force, that is, an airflow force on the motor scooter in the *x* and *y* directions, acted on the motor scooter carrying the dummy. Hereafter, as the motor scooter with the dummy was fixed to the frame through rigid rods with load cells, the force fluctuated from compression to tension and was damped to zero. The maximum resultant force was calculated by combining the *x*- and *y*-directional initial maximum compression forces, assuming that these forces were applied at the same time. The basis of this assumption is that the time difference between these two forces was <0.25 sec. Figure 7 shows the maximum resultant forces. Each case was repeatedly measured three times and the values were averaged. Unfortunately, the cases of distances of 1.5 m (4.92 ft) and 2.0 m (6.56 ft) at a trailer-tractor speed of 90 km/h (55.9 mph) could not be tested because of the restricted test-site conditions. The resultant forces almost linearly increased at low speeds as the distance decreased. As the speed increased to 80 km/h (49.7 mph) or higher, the resultant forces increased steeply as the distance decreased. This can be explained by introducing the concept of a boundary layer (16). As the tractor–trailer moves, an air velocity field develops around its solid surface. The air velocity becomes the speed of the tractor–trailer at the solid surface and becomes lower as the distance from the solid surface increases. As the speed of the tractor–trailer increases, the air velocity region, which is strongly affected by the tractor–trailer speed, extends. As this region extends, the force acting on the motor scooter with the dummy will be strongly influenced by the speed of the tractor–trailer. Considering the above results, we could conclude that there is a characteristic distance within which nearby objects can be strongly affected depending on the tractor–trailer speed. The resultant forces for a distance of 1.0 m (3.28 ft) between the motor scooter and the tractor–trailer

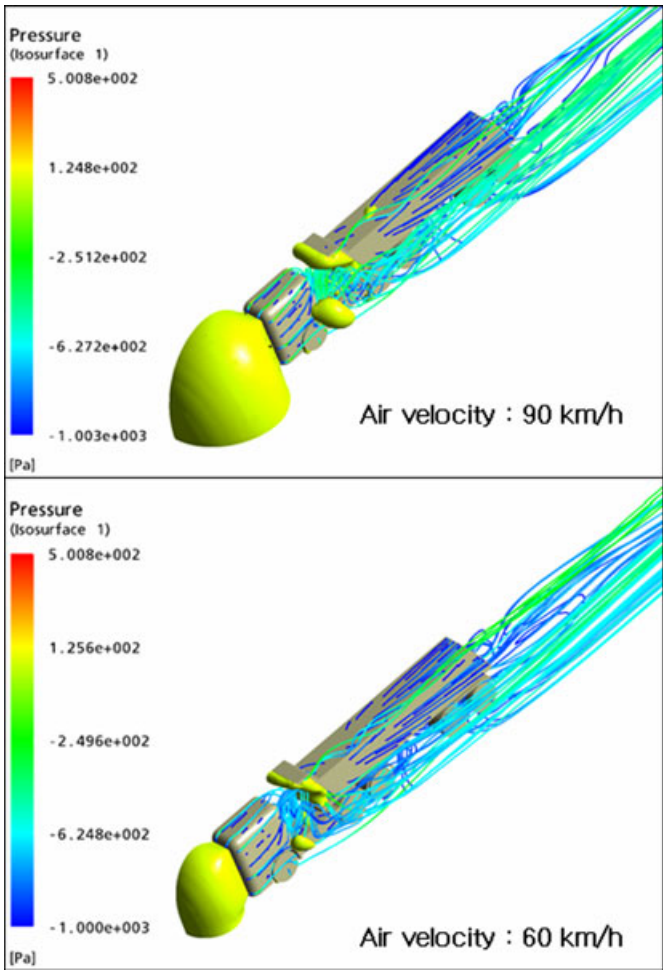

FIG. 8—*The results of flow analysis using the CFX program. Flow separation occurs at the front and back of the trailer. Because of the separation at the front of the trailer, the air flows separate, and this can increase the drag force on the motor scooter with the operator.*

were 87.8 N (19.7 lb) at a speed of 80 km/h (49.7 mph) and 124.5 N (28 lb) at a speed of 90 km/h (55.9 mph). These forces could abruptly disrupt the stability in maneuvering by an operator who is unaware of the approaching tractor–trailer.

Figure 8 shows the results of a flow analysis using the CFX program. Flow separation occurs at the front and back of the trailer. Because of the separation at the front of the trailer, the air flows separate, and this can increase the drag force on the motor scooter with the operator. As the air velocity increases, flow separation at the front face of the trailer and the domain of positive pressure at the front face of the tractor increases.

The drag coefficients are calculated using Eq. (1), where F_d is the maximum resultant force calculated from Fig. 7, ρ is the air density at 20°C (68°F), V is the speed of the trailer-tractor, and A is the cross-sectional area of the motor scooter with the dummy. The Reynolds number (Re), corresponding to the calculated drag coefficient, is calculated as follows (16):

$$\mathrm{Re} = \frac{\rho V L}{\mu} \tag{3}$$

where L is the characteristic length and μ is the air viscosity at 20°C (68°F). The characteristic length, L, is expressed as the front

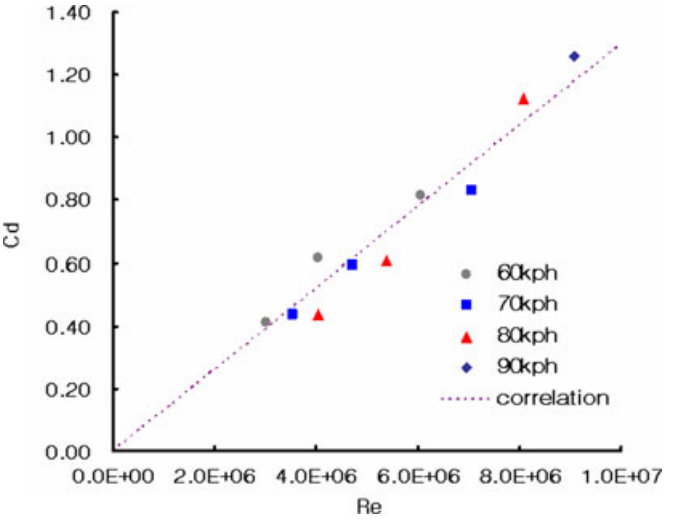

FIG. 9—*Comparison of the drag coefficient with the correlation. The two sets of drag coefficients are in good agreement, with a maximum deviation of 17%.*

cross-sectional area of the tractor–trailer divided by the distance to the motor scooter. Figure 9 displays the calculated drag coefficients versus the calculated Reynolds numbers. The points plotted as circles, rectangles, triangles, and diamonds represent the calculated drag coefficients at the corresponding calculated Reynolds numbers. From Fig. 9, the calculated drag coefficient can be expressed in terms of the dimensionless Reynolds number (Re) as follows:

$$C_d = 1.298 \times 10^{-7}\,\mathrm{Re} \tag{4}$$

Figure 9 also shows a comparison between the drag coefficients from Eq. (1) and those from Eq. (4), which are represented by the dashed line. The two sets of drag coefficients are in good agreement, with a maximum deviation of 17%. From the previous results, we have concluded that the drag force caused by the tractor–trailer can be expressed through the Reynolds number.

The current report has been carried out only for the specific case of an accident involving a tractor–trailer and a motor scooter. We plan to undertake further work considering various vehicles and relative objects, including pedestrians, to generalize the correlation.

References

1. Baker JS, Fricke LB. The traffic-accident investigation manual, 9th rev edn. Evanston, IL: Northwestern University Traffic Institute, 1986.
2. French AP. Newtonian mechanics, 1st rev edn. New York, NY: Norton & Company, 1970.
3. Xiu-Ling W, Guo-Qiang W, Su-Li F. Aerodynamic characteristics about mining dump truck and the improvement of head shape. J Hydrodynamics 2008;20(6):713–8.
4. Wang D, Du G, Wu J. Numerical experimental study on the 3-D flow field around a van with a dome for energy saving. Energy Convers Manag 2005;46:833–46.
5. Roy S, Srinivasan P. External flow analysis of a truck for drag reduction. SAE International Technical Paper Series, No. 2000-01-3500, http://papers.sae.org/2000-01-3500.
6. Cooper KR, Leuschen J. Model and full-scale wind tunnel tests of second-generation aerodynamic fuel saving devices for tractor-trailers. SAE International Technical Paper Series, No. 2005-01-3512, http://papers.sae.org/2005-01-3512.
7. Bettle J, Hollyway AGL, Venart JES. A computational study of the aerodynamic forces acting on a tractor-trailer vehicle on a bridge in cross-wind. J Wind Eng Ind Aerodyn 2003;91:573–92.

8. Pinelli JP, Subramanian C, Plamondon M. Wind effects on emergency vehicles. J Wind Eng Ind Aerodyn 2004;92:663–85.
9. Noger C, Regardin C, Szechenyi E. Investigation of the transient aerodynamics phenomena associated with passing manoeuvres. J Fluids Struct 2005;21:231–41.
10. Al-Garni AM, Bernal LP. Experimental study of a pickup truck near wake. J Wind Eng Ind Aerodyn 2010;98:100–12.
11. Watkins S, Vino G. The effect of vehicle spacing on the aerodynamics of a representative car shape. J Wind Eng Ind Aerodyn 2008;96: 1232–9.
12. Li L, Guang-Sheng D, Zheng-Gang L, Li L. The transient aerodynamic characteristics around vans running into a road tunnel. J Hydrodynamics 2010;22(2):283–8.
13. San-Andres A, Santiago-Prowald AJ. Train-induced pressure on pedestrians. J Wind Eng Ind Aerodyn 2002;90:1007–15.
14. Fricke LB. Traffic accident reconstruction, 1st rev edn. Evanston, IL: Northwestern University Traffic Institute, 1990.
15. ANSYS Inc. CFX-12 user manual. Canonsburg, PA: ANSYS Inc, 2009.
16. Fox RW, McDonald AT. Introduction to fluid mechanics, 5th rev edn. Singapore: John Wiley & Sons, 1998.

Additional information and reprint requests:
Chan-Seong Park, Ph.D.
Department of Physical Engineering
Central District Office of National Institute of Scientific Investigation
58-2, Hwa-Am Dong
Yusung Ku, Daejeon 305-348
Korea
E-mail: color@korea.kr